Fundamentally, PSR (m) is defined by

$$\rho = c(t_u - t_s) \quad ,$$

where c is the speed of propagation (m/s), t_u is the received time (s), and t_s is the transmitted time. An alternative expression for PSR is

$$\rho(t) = | \boldsymbol{r}_s(t) - \boldsymbol{r}_u(t) | + \varepsilon_\rho(t) \quad ,$$

where bold letters represent vectors, $\boldsymbol{r}_s$ is the position of the satellite, $\boldsymbol{r}_u$ is the position of the user receiver, $| \boldsymbol{r}_s - \boldsymbol{r}_u |$ is the geometric range between the two positions, and ε_ρ is the PSR error (m).

ADR is derived from the delta-PSR (DPSR) velocity measurement. The DPSR is defined by the rate of change of PSR (m/s)

$$\delta(t) = [\, \boldsymbol{v}_s(t) - \boldsymbol{v}_u(t)] \cdot \boldsymbol{1}(t) + \varepsilon_\delta(t) \quad ,$$

where $\boldsymbol{v}_s$ is the velocity of the satellite (m/s), $\boldsymbol{v}_u$ is the velocity of the receiver, ε_δ is the DPSR error, and $\boldsymbol{1}$ is the unit range vector between the satellite and the receiver defined by

$$\boldsymbol{1}(t) = \frac{\boldsymbol{r}_s(t) - \boldsymbol{r}_u(t)}{| \boldsymbol{r}_s(t) - \boldsymbol{r}_u(t) |} \quad .$$

DPSR can also be expressed as a function of Doppler frequency shift D (Hz) since

$$\lambda D(t) = [\mathbf{v}_s(t) - \mathbf{v}_u(t)] \cdot \mathbf{1}(t) \, ,$$

where λ is the carrier frequency wavelength (m). Substitution gives

$$\delta(t) = \lambda D(t) + \varepsilon_\delta(t) \quad .$$

Integrating DPSR yields ADR formally defined as

$$\alpha(t_1, t) = \int_{t_1}^{t} \delta(\tau) d\tau = | \boldsymbol{r}_s(t) - \boldsymbol{r}_u(t) | + \varepsilon_\alpha(t_1, t) \quad ,$$

where t_1 is the integration starting time and ADR error is related to DPSR error via

$$\varepsilon_\alpha(t_1, t) = \int_{t_1}^{t} \varepsilon_\delta(\tau) d\tau \quad ,$$

Finally, CMC is formally defined as

$$\chi(t_1,t) = \rho(t) - \alpha(t_1,t) \quad .$$

CMC minimizes systematic errors common to both PSR and ADR and helps isolate the effects of interference.

Examples of simulated PSR, DPSR, ADR, and CMC are shown in Figure 5.3.1.1. These parameters are taken from the simulator "log" file which provides true range data used to calculate range error in the next section. Simulation time is the time from the start of the simulation. PSR is from approximately 20.4×10^6 m to 20.8×10^6 m. The satellite is at zenith when the PSR is a minimum at approximately 1300 s. DPSR is a relatively straight line with negative velocities as the satellite approaches and positive velocities as it recedes. The DPSR is 0 m/s at zenith corresponding to a 0-Hz Doppler shift. ADR is 0 m at the start of the simulation. The ADR decreases as the satellite approaches and increases as the satellite recedes. The ADR curve is similar to the PSR curve without the initial range offset. CMC is constant at this offset from start to finish.

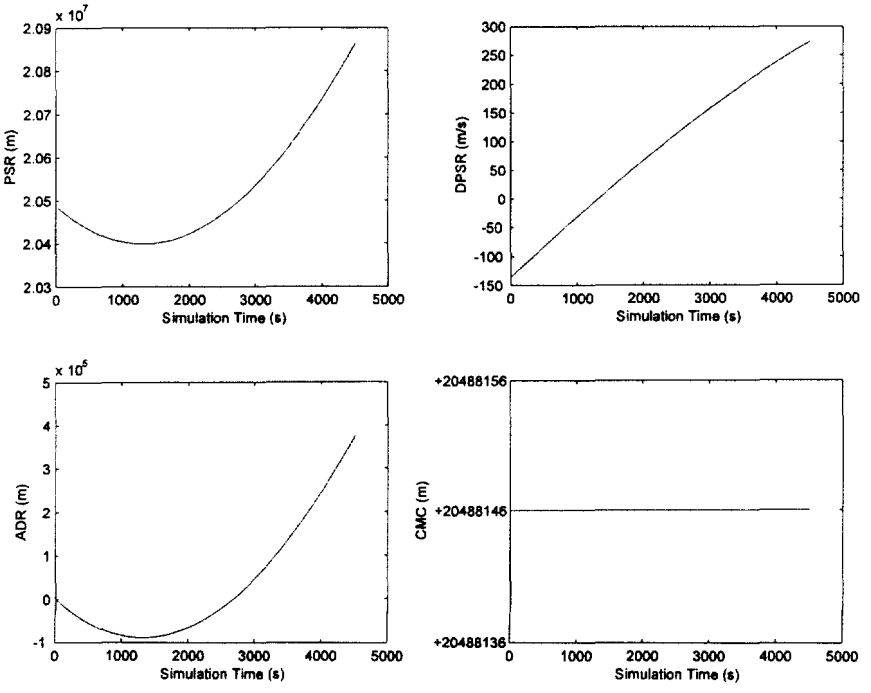

Figure 5.3.1.1 Simulated values.

Range Error

Measured ranges have more sources of error than simulated ranges [5, 6]. For example, measured PSR is represented by

$$\hat{\rho}(t) = \left| \boldsymbol{r}_s(t) - \boldsymbol{r}_u(t) \right| + c\hat{b}_u(t) + \hat{\varepsilon}_\rho(t) \quad ,$$

where $\hat{}$ denotes measured values and b_u is the receiver clock offset (s). This expression demonstrates that measured ranges are influenced by receiver noise and clock inaccuracies. These error sources are also present in DPSR as expressed by

$$\hat{\delta}(t) = \lambda \hat{D}(t) + c\frac{d\hat{b}_u(t)}{dt} + \hat{\varepsilon}_\delta(t)$$

and consequently ADR. Computation of ADR alone sometimes requires compensation of the clock offset for Doppler effects. Computation of ADR for CMC does not require this compensation because these effects are also present in PSR.

Examples of measured PSR, DPSR, ADR, and CMC are shown in Figure 5.3.1.2. These parameters were measured using Rx 1 with -93 dBm/20MHz Gaussian noise added to the GPS signal. The measured ranges are different from the simulated ranges in Figure 5.3.1.1. CMC shows measurement uncertainty most dramatically because systematic error was removed.

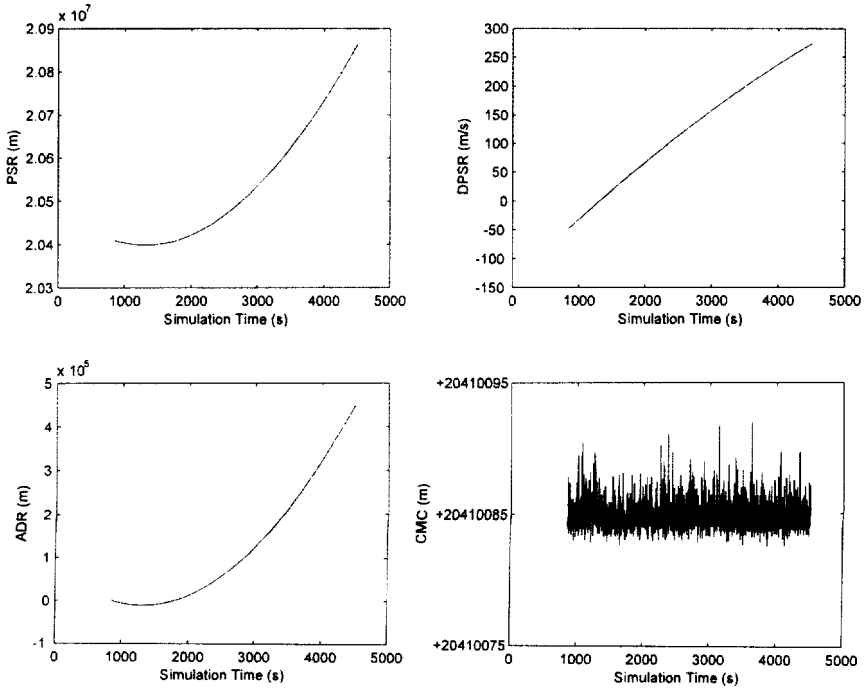

Figure 5.3.1.2 Reference measurement values.

Range error is the difference between simulated and measured range estimates. PSR error is

$$\Delta_\rho(t) = \hat{\rho}(t) - c\hat{b}_u(t) - \rho(t) = \hat{\varepsilon}_\rho(t) - \varepsilon_\rho(t) \quad ,$$

ADR error is

$$\Delta_\alpha(t_1,t) = \hat{\alpha}(t_1,t) - \alpha(t_1,t) = \hat{\varepsilon}_\alpha(t_1,t) - \varepsilon_\alpha(t_1,t) \quad ,$$

and CMC error is

$$\Delta_\chi(t_1,t) = \hat{\chi}(t_1,t) - \chi(t_1,t) = [\hat{\varepsilon}_\rho(t) - \varepsilon_\rho(t)] - [\hat{\varepsilon}_\alpha(t_1,t) - \varepsilon_\alpha(t_1,t)] \quad .$$

Figure 5.3.1.3 shows range error corresponding to the simulated and measured ranges in Figures 5.3.1.1 and 5.3.1.2. Notice that PSR and ADR cases have curved features while the CMC case is relatively flat. The curves are indicative of an underlying non-stationary process where the range-error statistic is dependent on time. This non-stationarity is undesirable and must be minimized before more detailed statistical analysis can proceed.

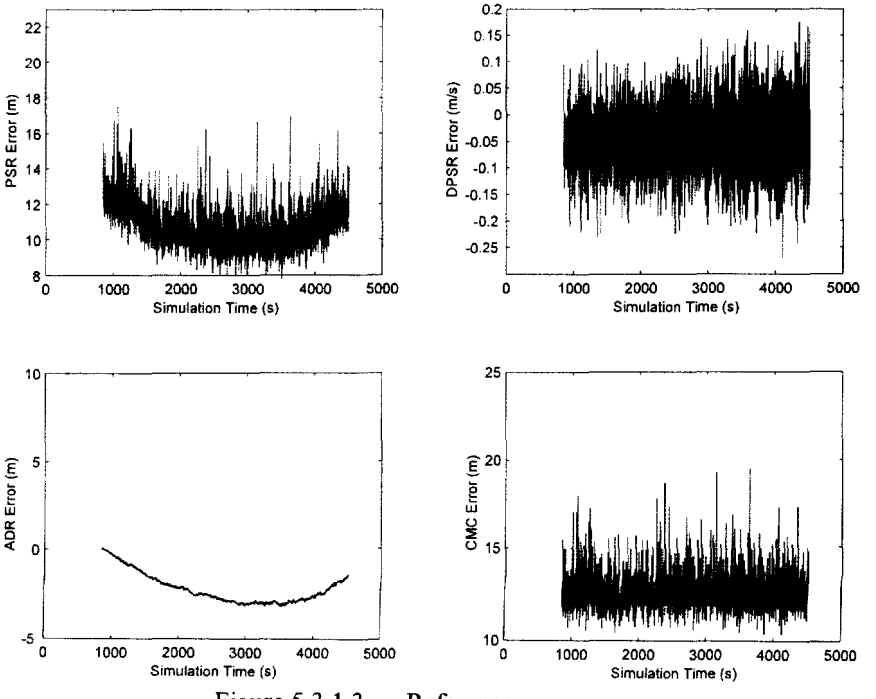

Figure 5.3.1.3 Reference range error.

Range error residual

In order to separate the effects of UWB interference, a general expression for range error is

$$\Delta = \Delta_{ref} + \hat{\varepsilon}_{UWB} \quad ,$$

where the Δ_{ref} is the reference range error and $\hat{\epsilon}_{UWB}$ is error introduced by UWB interference. We measure Δ_{ref} under nominal SNR conditions specified in Table 4.1.1. Figures 5.3.1.2 and 5.3.1.3 show the reference range and reference range error for Rx 1, respectively.

The reference range error can be modeled as

$$\Delta_{ref} = \Phi_{ref} + \varphi_{ref} \quad ,$$

where Φ_{ref} represents the non-stationary systematic reference error and φ_{ref} represents the random reference error and contains high-order components of Δ_{ref}. Φ_{ref} is a function derived from a 3rd order polynomial fit to Δ_{ref}. Figures 5.3.1.4 and 5.3.1.5 show these errors for Rx 1. Subtracting Φ_{ref} from Δ_{ref} removes non-stationary systematic error and yields a range error residual

$$\gamma = \Delta - \Phi_{ref}^{(3)} = \hat{\varepsilon}_{UWB} + \varphi_{ref} \quad ,$$

which is our best estimate to range error due to UWB interference.

Figures 5.3.1.6 and 5.3.1.7 show systematic along with measured range error for two different UWB interference signals. The first is 1-MHz PRF with UPS and no gating. The second is 1-MHz PRF with 2% RRD and no gating. In both cases, Rx 1 was exposed to the maximum UWB power levels where lock is maintained. The UPS case has spectral line interference starting at 2000 seconds. PSR, ADR, and CMC show significant changes in error at this point. Prior to this spectral alignment, the error coincides with Φ_{ref}. The 2% RRD case has an elevated range error when compared to Φ_{ref}.

Figures 5.3.1.8 and 5.3.1.9 show the range error residuals for these same UWB signals. Clearly the magnitude of the residuals is less. The increased error due to spectral line interference is still dominant in the UPS case.

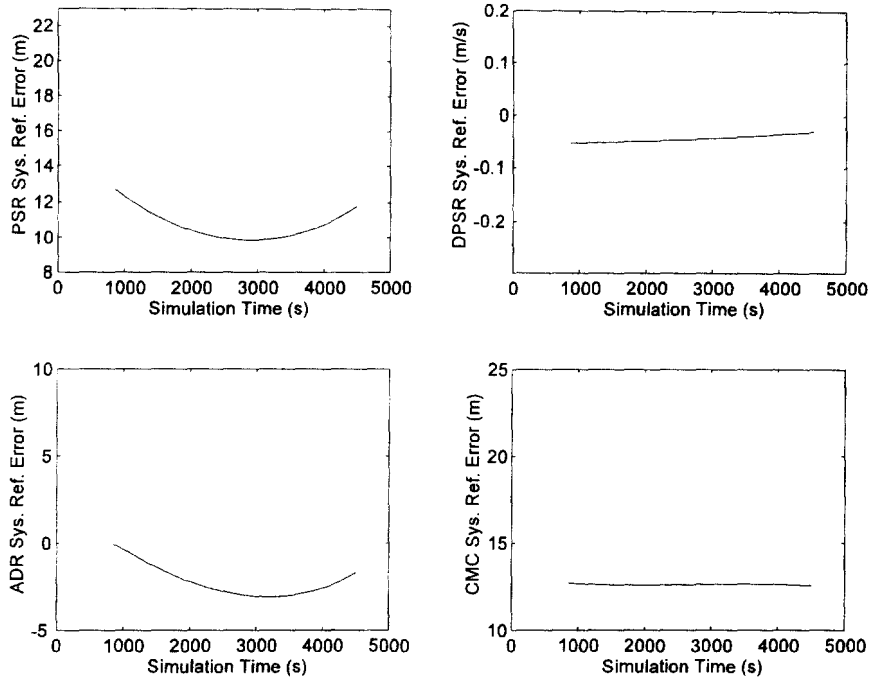

Figure 5.3.1.4 Systematic reference error (Φ_{ref}).

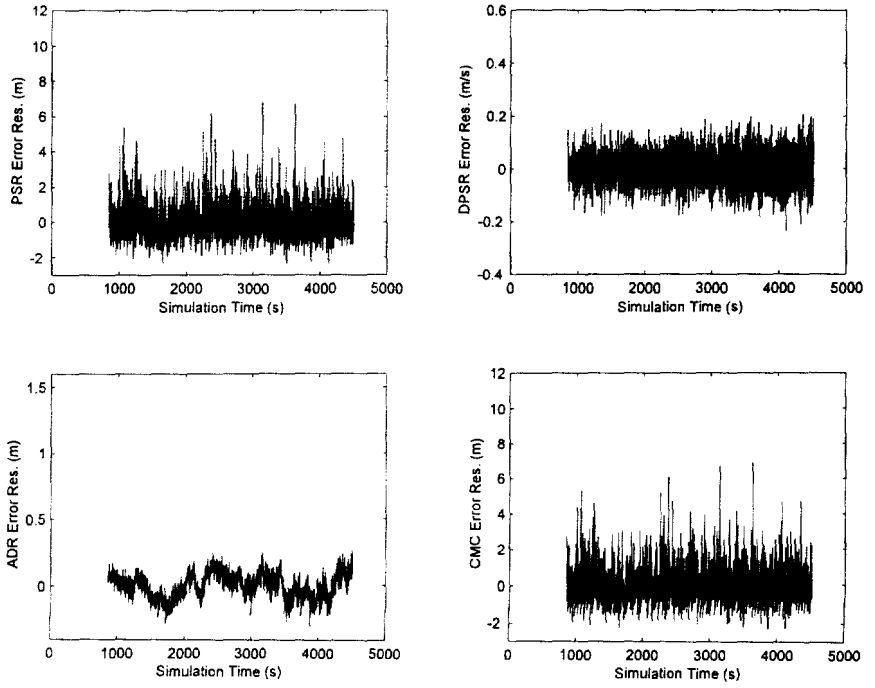

Figure 5.3.1.5 Random reference error (φ_{ref}).

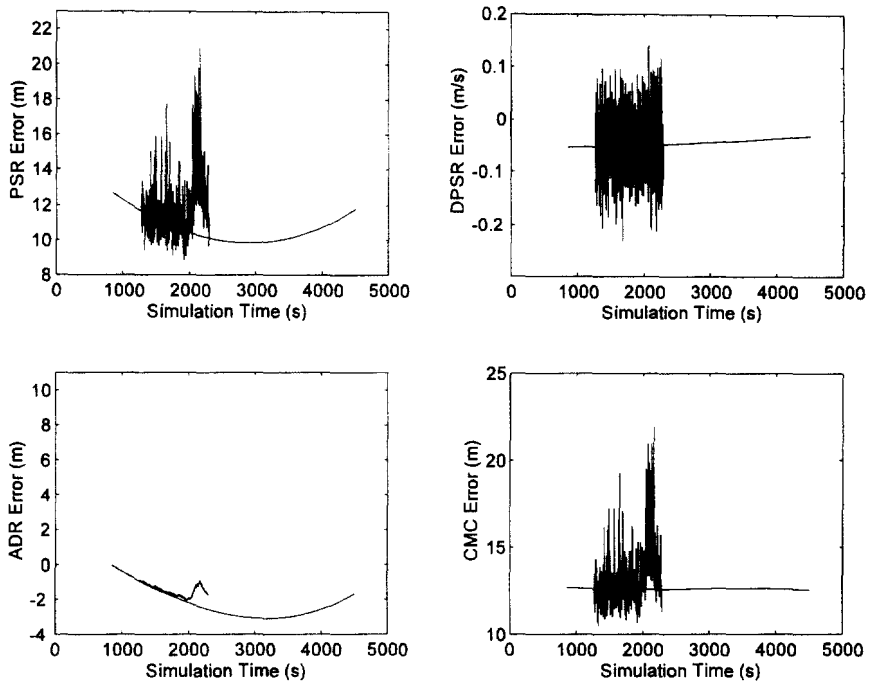

Figure 5.3.1.6 Range error due to 1-MHz PRF with UPS interference compared to systematic reference range error.

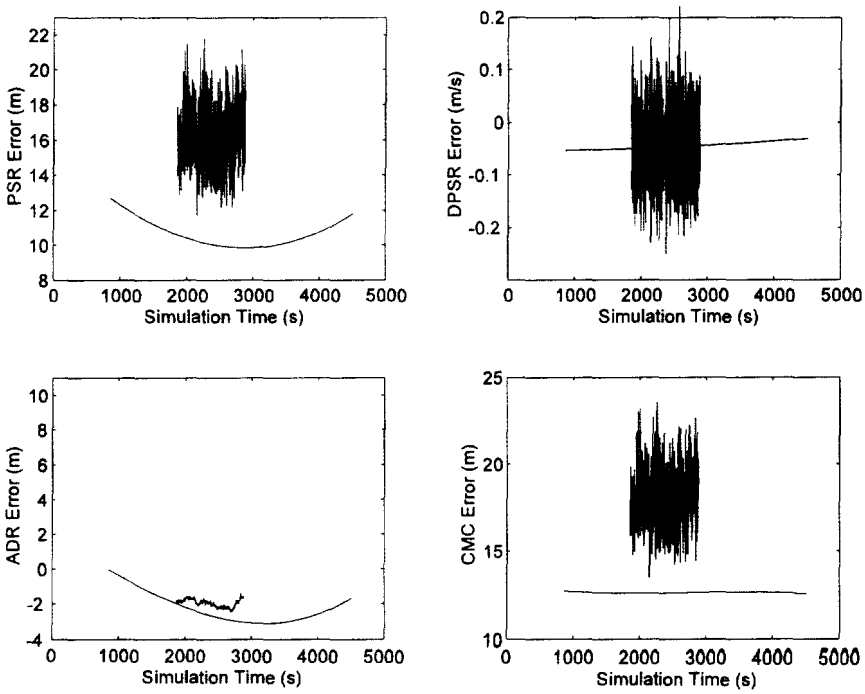

Figure 5.3.1.7 Range error due to 1-MHz PRF with 2%-RRD interference compared to systematic reference range error.

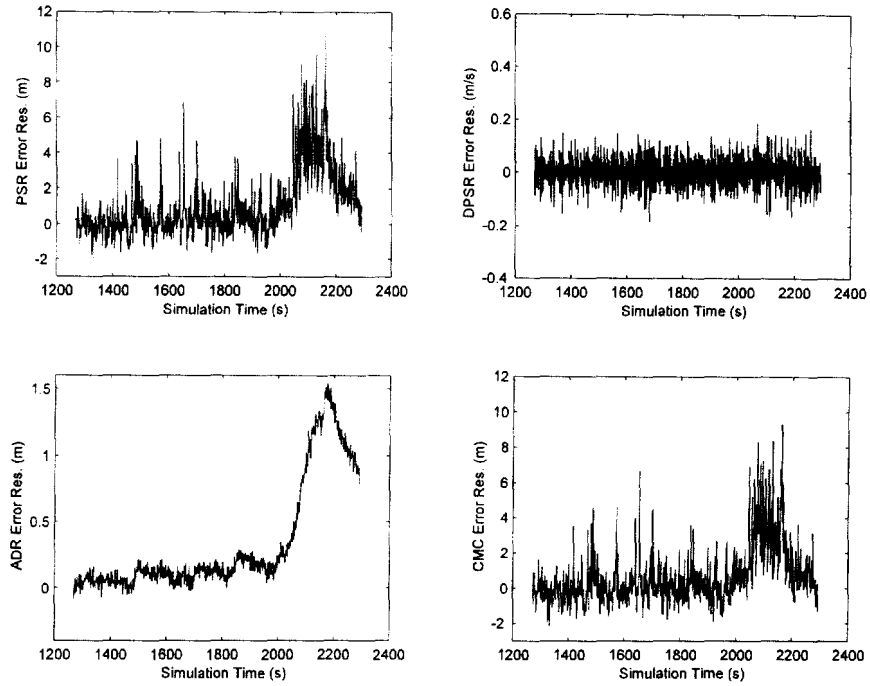

Figure 5.3.1.8 Range error residual due to 1-MHz PRF with UPS interference.

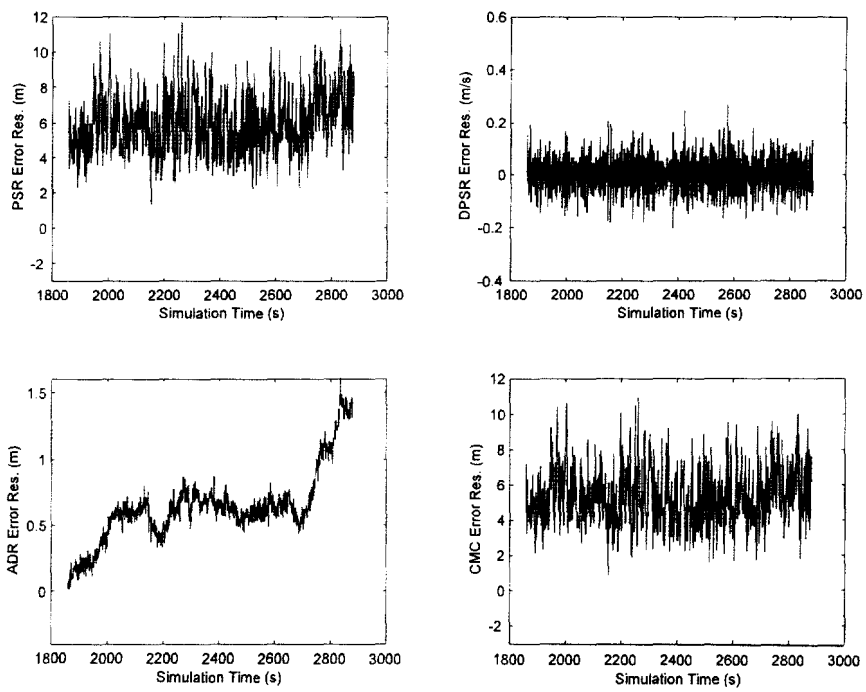

Figure 5.3.1.9 Range error residual due to 1-MHz PRF, 2%-RRD interference.

Range error residual statistics

The range error residual is analyzed with numerous statistics. Range error residual standard deviation is a commonly used statistic for evaluating the effect of interference. Zero-mean, Gaussian distributed random variables are completely described by the standard deviation statistic

$$\sigma_\gamma = \sqrt{\frac{1}{N}\sum_{n=1}^{N}(\gamma_n - m_\gamma)^2} \quad .$$

where N is the number of range error residual samples and m is the mean range error residual. Although this statistic was evaluated, it was deemed insufficient because the range error residuals were often non-Gaussian. Therefore, in addition to standard deviation, other statistics including percentiles were analyzed [7].

Percentiles are computed from the CDF defined by

$$F_\Gamma(\gamma) = P(\Gamma \le \gamma) \quad ,$$

where Γ is the range error residual random variable. The CDF is most easily obtained by sorting the sampled γ into ascending values. The probability corresponds to the position in the sorted array. The median, 84th, and 98th percentiles represent the range error residual value that are greater than or equal to all others 50, 84, and 98% of the time. The 84th and 98th percentiles are significant because they represent the 1 and 2 standard deviation values for a zero-mean Gaussian distributed random variable.

Figures 5.3.1.10, 5.3.1.11, and 5.3.1.12 show the range error residual CDFs of the reference measurement and the two 1-MHz PRF cases described above. These CDFs are plotted on a Gaussian graph where a Gaussian distributed random variable is represented by a positively sloped, straight line. The UPS case deviates from this line at approximately the 84th percentile. This percentile corresponds to the time the spectral line interference is present during the BL measurement. The CDF of the 2% RRD case appears Gaussian. The percentiles for PSR and CMC track each other in both cases. This is to be expected since CMC error is dominated by PSR error.

The skewness, excess, and median-to-mean ratio statistics quantify the "Gaussian-ness" of the range error residual. The skewness measures the symmetry of a probability density function and is defined by

$$\beta_1 = \frac{1}{\sigma^3}\sqrt{\frac{1}{N}\sum_{n=1}^{N}(\gamma_n - m_\gamma)^3} \quad .$$

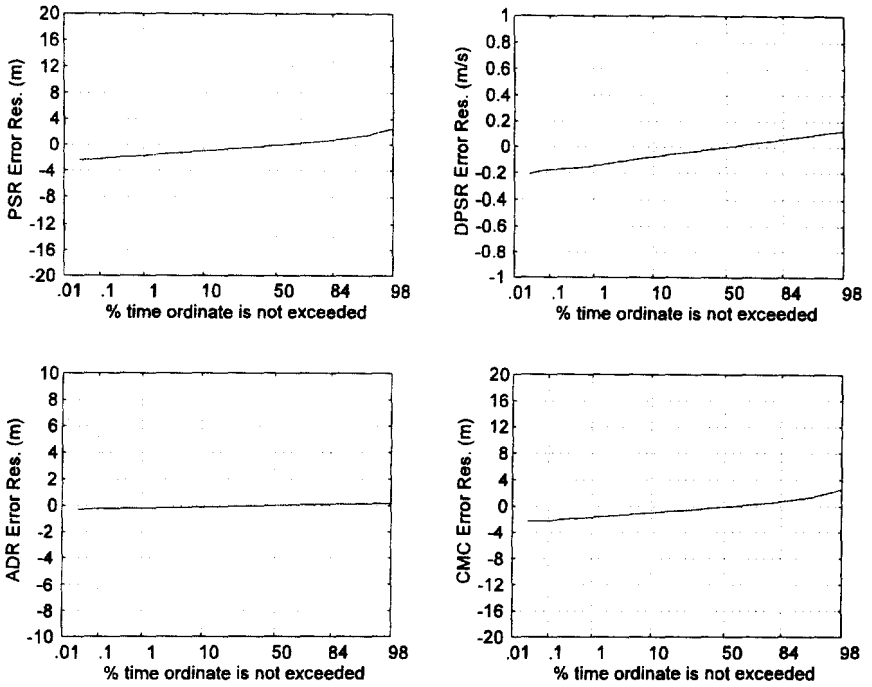

Figure 5.3.1.10 Reference range error residual CDF.

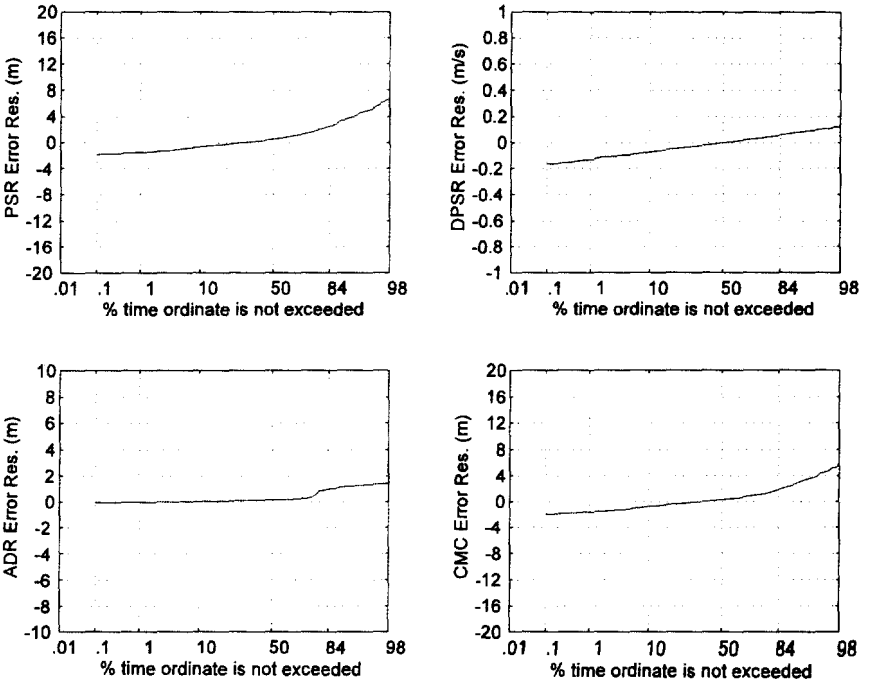

Figure 5.3.1.11 Range error residual CDF for 1-MHz PRF with UPS interference measurement.

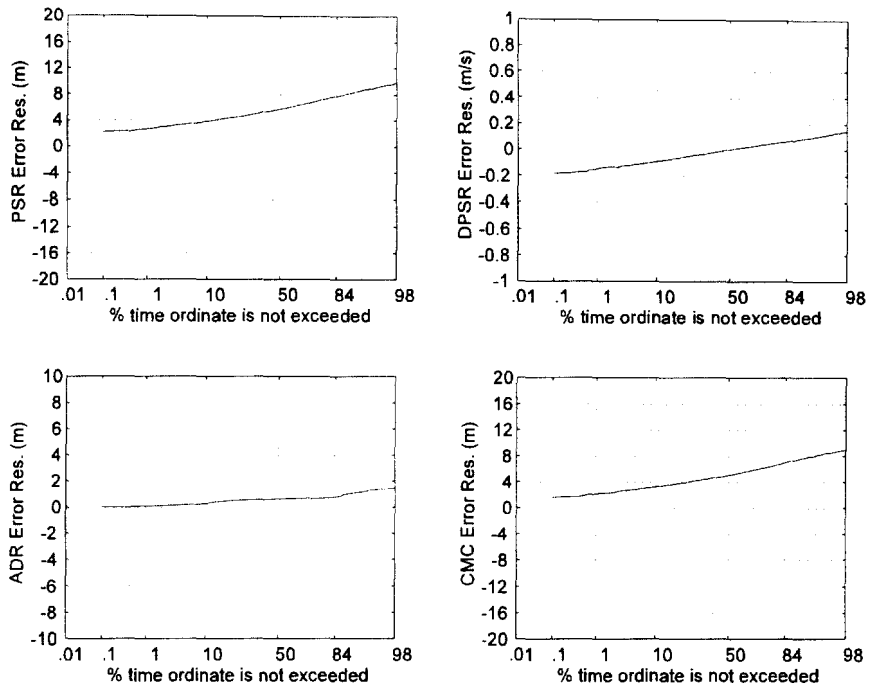

Figure 5.3.1.12 Range error residual CDF for 1-MHz PRF with 2% RRD interference measurement.

Gaussian distributed random variables have a skewness of 0. The excess measures the "peakedness" of a random variable and is defined by

$$\beta_2 = \frac{1}{\sigma^4}\sqrt{\frac{1}{N}\sum_{n=1}^{N}(\gamma_n - m_\gamma)^4} \quad .$$

Gaussian distributed random variables have an excess of 3. A Gaussian distributed random variable has a median-to-mean ratio of 1. For display, 3 is subtracted from excess and 1 is subtracted from the median-to-mean ratio so they, like skewness, will be centered at zero. Deviations from zero for any of these statistics will indicate that the random variable is non-Gaussian.

Range error residual standard deviation estimates are unreliable if there are too few independent samples. The auto-correlation function is used to evaluate the independence of the range error residual samples:

$$R_\Gamma(k) = \sum_{n=1}^{N}(\gamma_n - m_\gamma)(\gamma_{n+k} - m_\gamma) \quad ,$$

where m_γ represents the mean residual error and N is the number of residual error samples. The number of correlated samples is the smallest value of k whose autocorrelation is less than $R(0)/2$. ADR error residuals were typically highly correlated because ADR is the result of integrating DPSR. Figures 5.3.1.13, 5.3.1.14, and 5.3.1.15 show the autocorrelation function of the reference measurement, UPS case, and 2% RRD case. The reference measurement and 2% RRD case show clear independence between observations. The UPS case shows more correlation corresponding to the length of time spent with and without line interference.

5.3.2 Cycle Slip and Signal-to-Noise Ratio

To our knowledge, the receivers that were tested do not count or estimate the actual number of cycle slips. Instead, the receivers monitor parameters that are correlated to cycle slip conditions (e.g., SNR, carrier phase lock, and bit error rates).

Cycle slip condition is a binomially distributed random variable, being either present or not. Analysis consists of counting the number of observations where cycle slip conditions are present and dividing by the total number of observations. This fraction represents cycle slip condition probability which is converted to percentage for display.

Figures 5.3.2.1a and 5.3.2.2a show cycle slip condition probability for the two 1-MHz PRF cases described above. The UPS case has the majority of cycle slip conditions clustered around the time when line interference is strongest. For the 2% RRD case, cycle slip conditions are scattered uniformly throughout the entire measurement.

SNR is analyzed in percentiles in a similar manner to the range error residual. The occurrence of low SNR is of interest thus the 50th, 16th, and 2nd percentiles are displayed. Figures 5.3.2.1b and 5.3.2.2b show SNR behavior for the two 1-MHz PRF cases. As expected, the UPS case has degraded SNR around the time when line interference is strongest. The 2% RRD case has small degradations in SNR throughout the entire measurement.

It should be noted that GPS receiver SNR measurements may not be accurate when the band-limited UWB signal has non-Gaussian statistics. The designer of the GPS noise measurement circuitry may have assumed, for example, that the noise would have Gaussian statistics. Thus, the SNR threshold for cycle slip conditions may need to be adjusted for non-Gaussian noise.

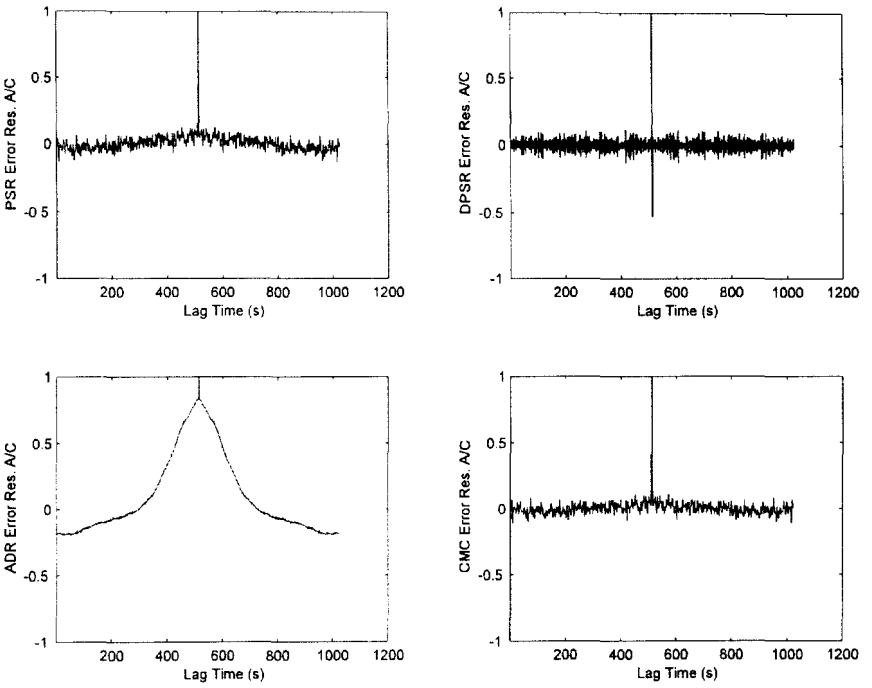

Figure 5.3.1.13 Autocorrelation of reference range error residual.

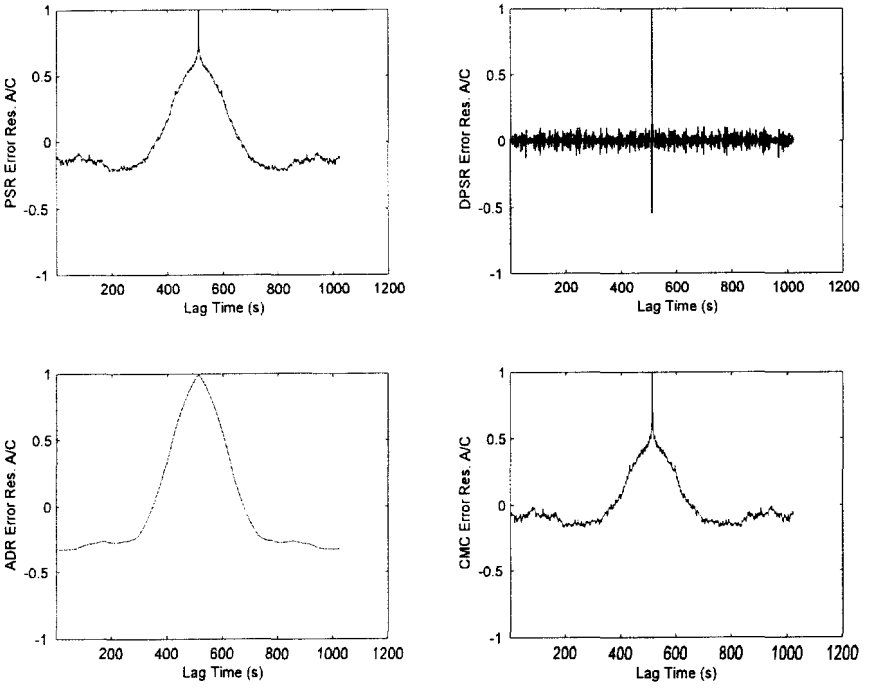

Figure 5.3.1.14 Autocorrelation of range error residual for 1-MHz PRF with UPS interference measurement.

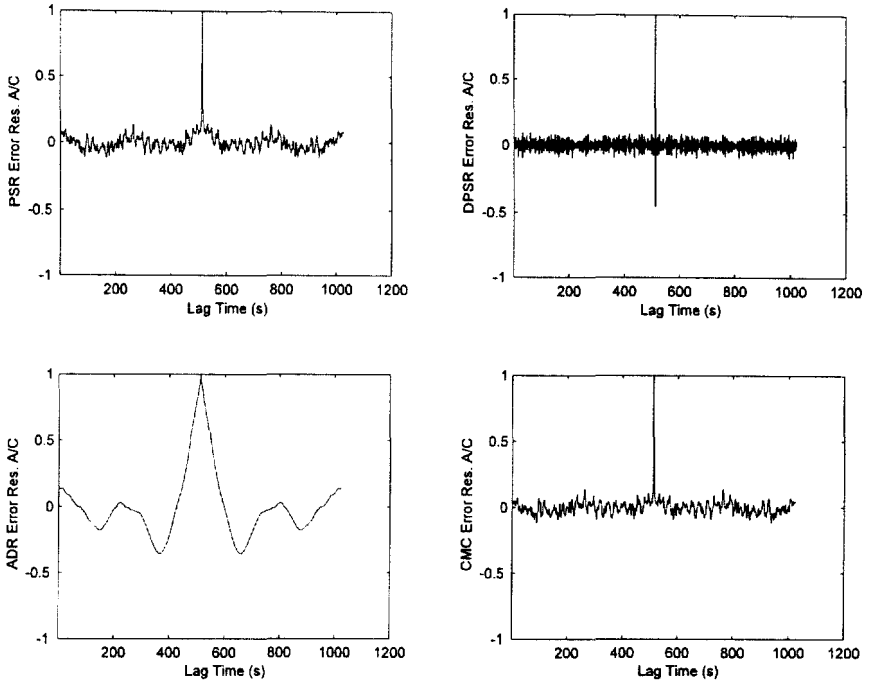

Figure 5.3.1.15 Autocorrelation for 1-MHz PRF with 2%-RRD interference measurement.

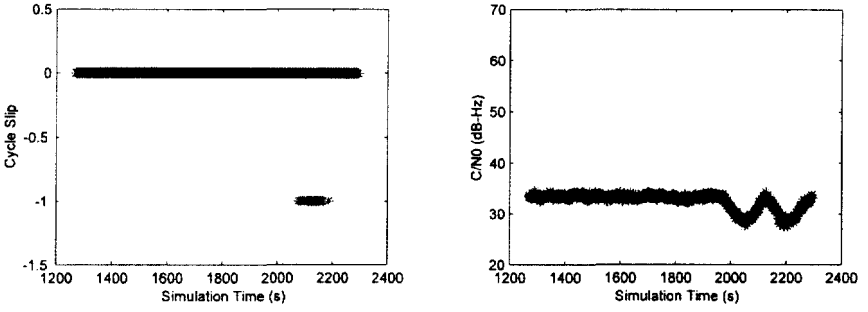

Figure 5.3.2.1 Cycle slips and SNR for 1-MHz PRF with UPS interference measurement.

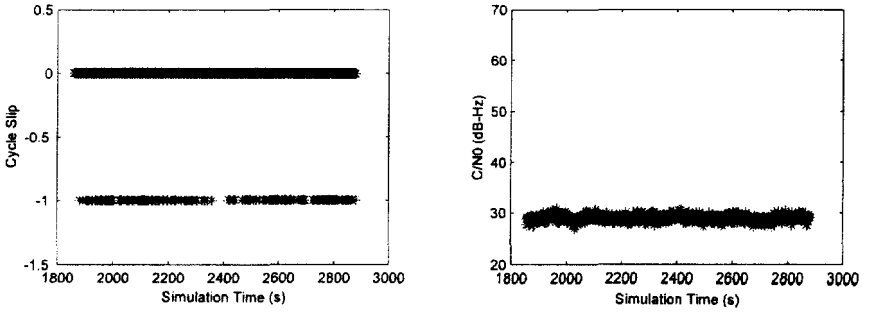

Figure 5.3.2.2 Cycle slips and SNR for 1-MHz PRF with 2%-RRD interference measurement.

5.4 Uncertainty Analysis

Four random variables are estimated through measurement: BL point, RQT, range error, and probability of cycle slip conditions. Discussion of the uncertainty of these estimates is as important as the estimates themselves.

Uncertainty is often quoted in terms of accuracy and precision. An accurate estimate implies that the mean is close to the true value. A precise estimate implies that the variation about the mean is minimal. Another way of expressing uncertainty is to define a random interval along with a probability or confidence that the random interval will include the true value [8].

5.4.1 Break-lock Point

BL point was found to occur as much as 4 dB below the UWB signal level that first caused BL. A test using Gaussian noise with Rx 1 showed that it was possible to have successful and unsuccessful BL measurements over a 4-dB range. Below this range BL was seldom experienced with repeated trials. Above this range BL was frequently experienced with repeated trials. Thus, it can be said that the BL point variability is approximately ±2 dB.

5.4.2 RQT

RQT is assumed to be Gaussian distributed. However, since there are a limited number of RQT trials the Student-t distribution is used for computational purposes. Formally, if the number of trials is fixed at 10, the confidence interval for 95% confidence is

$$m - 0.76s \leq u < m + 0.76s \quad ,$$

where u is the true mean, m is the measured mean, and s is the measured standard deviation. This uncertainty estimate is only valid when all trials had successful reacquisitions. RQT trials are considered independent because the receiver was reset at the beginning of each measurement.

5.4.3 Range Error

The standard deviation of the range error residual, σ_{uere}, (user-equivalent range error) is an important factor in the GPS error budget. The uncertainty of a laboratory estimate of σ_{uere} is often expressed as a confidence interval. If there are 1024 independent observations and the underlying process is Gaussian distributed, the standard deviation interval for 95% confidence is

$$0.9585s \leq \sigma < 1.045s \quad ,$$

where s is the measured range error residual standard deviation, and σ is the true range error residual standard deviation. Range error residual confidence intervals cannot be computed for UWB signals with spectral line interference because their statistics are non-Gaussian.

5.4.4 Cycle Slip Conditions

For Rx 1, cycle slip conditions do not cause loss of lock. Thus it was possible to collect a number of cycle slip condition samples during a single BL measurement. Although it is practical to compute the uncertainty of this random variable it is unclear how independent the cycle slip condition samples are. For example, if the cycle slip condition is detected with a message parity error it may take several seconds to clear the cycle slip condition indicator. Since cycle slips condition is used to support other trends it was deemed unnecessary to analyze the uncertainty of cycle slip condition probability.

6. RESULTS

This section discusses the measured characteristics of the various UWB interference sources, explains measured GPS operational and observational parameters, and summarizes trends.

6.1 UWB Spectral and Temporal Characteristics

In order to better understand the interference effects of UWB signals, it is helpful to understand their frequency and time-domain characteristics. A general description of the spectral features was given in Section 4.1.2. In this section, time-domain characteristics of the interfering signals are discussed.

When a narrow pulse, with a wide bandwidth (BW), is passed through a filter with a narrower bandwidth, the output is essentially equal to the impulse response of the filter and has a pulse width approximately equal to the reciprocal of the receiver bandwidth. Figure 6.1.1 illustrates 50%-ARD UWB signals, at three different PRFs, passed through a 20-MHz bandpass filter (center frequency of 1575.42 MHz) and downconverted to a center frequency of 321.4 MHz. The result is that, as the pulse passes through the filter, it becomes wider, the peak-to-average power decreases, and depending upon the PRF and extent of dithering, the pulses may overlap.

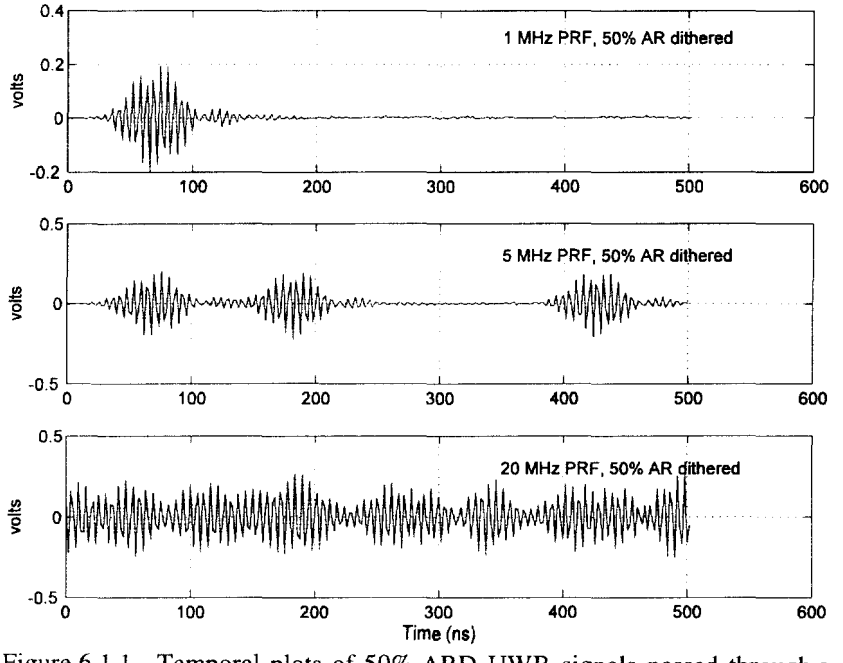

Figure 6.1.1. Temporal plots of 50%-ARD UWB signals passed through a 20-MHz bandpass filter and downconverted to a center frequency of 321.4 MHz.

One way to describe the time-domain characteristics is through APDs. These distributions are helpful for several reasons: when normalized to mean power, they can quickly show the relationship between peak, mean, and median power levels (as well as other percentiles); they reflect impulsiveness of the signal and the extent to which the signal power is present; they indicate the degree to which a signal is Gaussian; and they quickly distinguish signals that are constant amplitude in nature. APDs are particularly valuable, therefore, for providing statistical descriptions of wide bandwidth signals as they pass through the varying bandwidths of receivers. A tutorial on APDs is provided in Appendix E for those readers unfamiliar with their use.

A complete set of APDs, for each of the UWB signals used in these measurements, is provided in Appendix B. Additionally, a few composite APD plots are shown here for the purpose of illustration. For each of the composite plots, the mean power is normalized to 0 dBm so that the peak-to-average power can be readily determined. As a reference, an equivalent 0-dBm mean-power APD for Gaussian noise is plotted along with the UWB signals.

Figure 6.1.2 shows the normalized APDs for 8 different permutations of a UWB signal with a 100-kHz PRF. One can see that the amplitude distributions of the dithered signals are identical to the non-dithered cases. This is because, even for 50% ARD, the space between pulses is no less than 5 μs apart; since the UWB pulse width after passing through a 3-MHz filter is approximately 300 ns, the pulses remain discrete and never overlap.

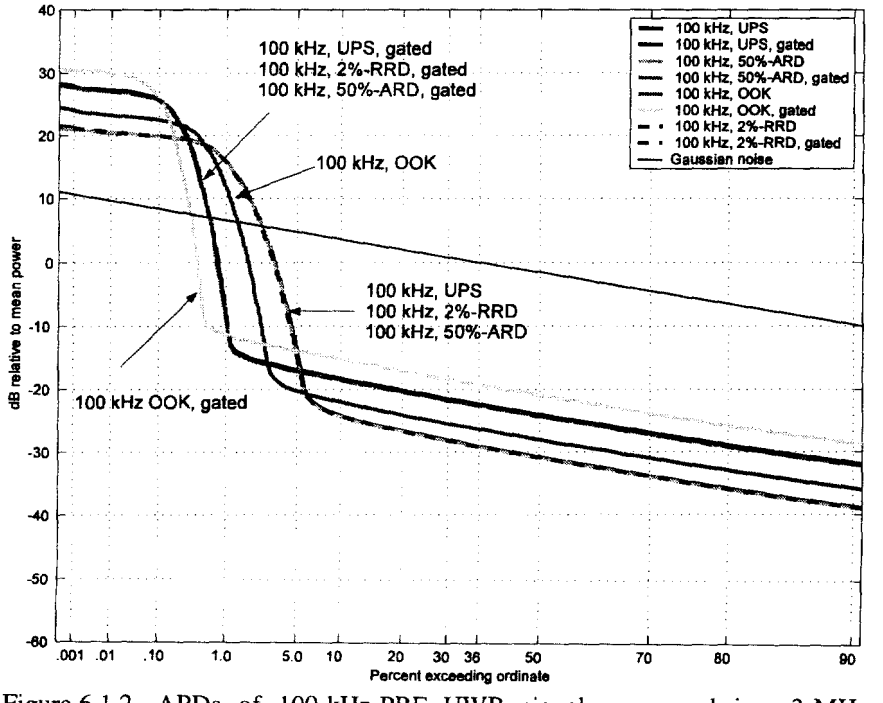

Figure 6.1.2. APDs of 100-kHz-PRF UWB signals measured in a 3-MHz bandwidth.

Therefore, while these dithered cases show a noise-like spectrum, they are non-Gaussian and impulsive with regard to their amplitude distributions.

Figure 6.1.3 shows the same plots for UWB signals with a PRF of 20 MHz. In this case, the UPS signal is sinusoidal (flat line), as we would expect since only one spectral line is allowed to pass through the 3-MHz filter. The dithered, non-gated cases, however, are Gaussian distributed. This is because the 20-MHz PRF is high enough to cause pulse overlap. Therefore, any random variations in the pulse spacing results in destructive and constructive addition of adjacent pulses and an apparent Gaussian distribution.

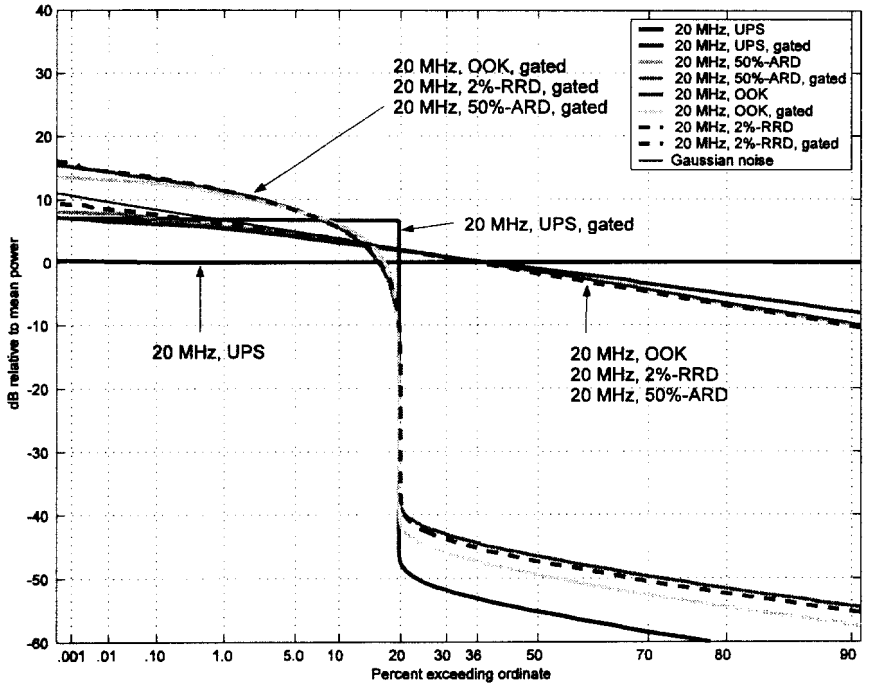

Figure 6.1.3. APDs of 20-MHz-PRF UWB signals measured in a 3-MHz bandwidth.

Figure 6.1.4 shows variations in amplitude distributions for 50% ARD pulses, varied with regard to PRF and passed through a 3-MHz bandwidth filter. One can see a natural progression as the pulses become more closely spaced: the pulse energy is present a greater percentage of the time, and as the pulses start to overlap, the signal amplitude distribution becomes more Gaussian-like.

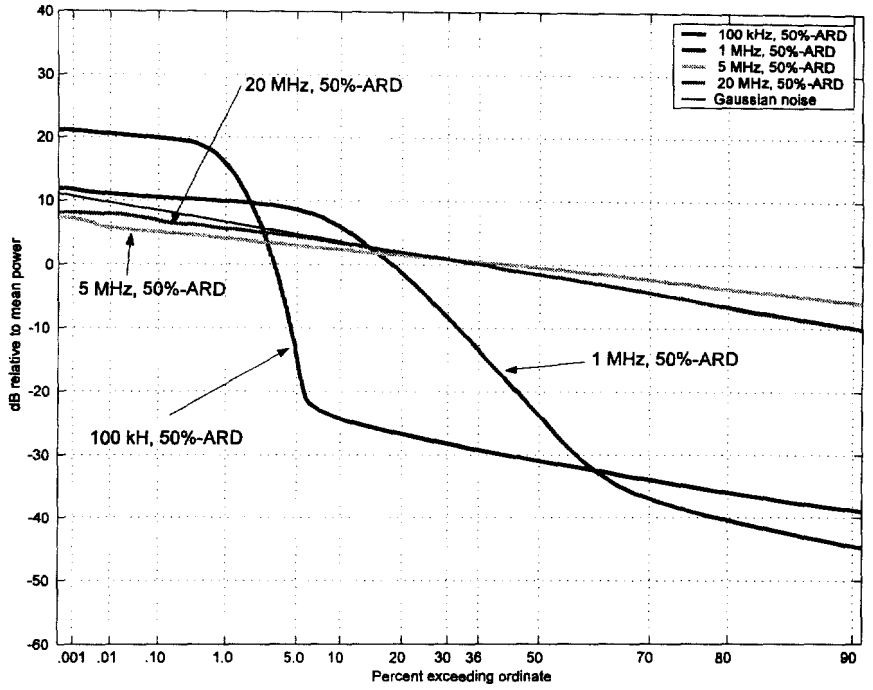

Figure 6.1.4. APDs of 50%-ARD UWB signals measured in a 3-MHz bandwidth.

6.2 GPS Interference Measurement Results

As discussed in the data analysis section, certain operational and observational metrics were chosen to demonstrate GPS receiver performance degradation. Results are given to establish how receivers respond to increasing levels of Gaussian noise with no UWB interference. Composite single-source and aggregate UWB results are provided to relate trends in GPS performance degradation to UWB interference parameters (e.g., PRF, pulse spacing). Whenever relevant, gated UWB results are plotted directly below non-gated UWB results to demonstrate the effects of gating. Table 6.2.1 gives a summary of the Figures under discussion in this section.

Table 6.2.1. Composite Figure List

Interference	Rx 1			Rx 2		
	BL	RQT	CMC	BL	RQT	CMC
Noise	6.2.1.1, 6.2.1.2	6.2.1.8	6.2.2.1	6.2.1.3, 6.2.1.4	6.2.1.8	N/A
UPS	6.2.1.1, 6.2.1.2	N/A	6.2.2.2	6.2.1.3, 6.2.1.4	N/A	N/A
OOK	6.2.1.1, 6.2.1.2	N/A	6.2.2.3	6.2.1.3, 6.2.1.4	N/A	N/A
2%-RRD	6.2.1.1, 6.2.1.2	6.2.1.9	6.2.2.4	6.2.1.3, 6.2.1.4	6.2.1.11	N/A
50%-ARD	6.2.1.1, 6.2.1.2	6.2.1.10	6.2.2.5	6.2.1.3, 6.2.1.4	6.2.1.12	N/A
Aggregate	6.2.1.7	6.2.1.13	6.2.2.6	N/A	N/A	N/A

Figures 6.2.1 through 6.2.5 are composite graphs showing the BL point for each of the UWB permutations. For those cases where no BL point is displayed, the receiver never lost lock. RQT results are given in Figures 6.2.6 through 6.2.11. CMC residual-error standard deviation was chosen to demonstrate UWB interference effects and is plotted in Figures 6.2.12 through 6.2.16.

In addition, Appendix F provides a comprehensive set of plots – each set summarizing results for type of UWB interference to a specific receiver. The plots on the left side pertain to the code-tracking loop and display CMC statistics (recall that CMC statistics are dominated by PSR statistics). Error-residual percentiles and standard deviation are shown on the upper left, and measures to quantify skewness, excess, and independence are given on the lower left. The upper-right plots provide information pertaining to carrier-loop tracking such as ADR percentiles and cycle slip conditions. Often, cycle slip conditions correlate to SNR estimated by the receiver. SNR percentiles are given with RQT data on the lower right.

The various graphs show parameter effects as a function of signal power for each of the UWB permutations. The reader is referred to Table 4.1.1 for Gaussian noise power level settings for each receiver. Also the power of all gated signals is expressed as the average power during the on-time of the gated cycle.

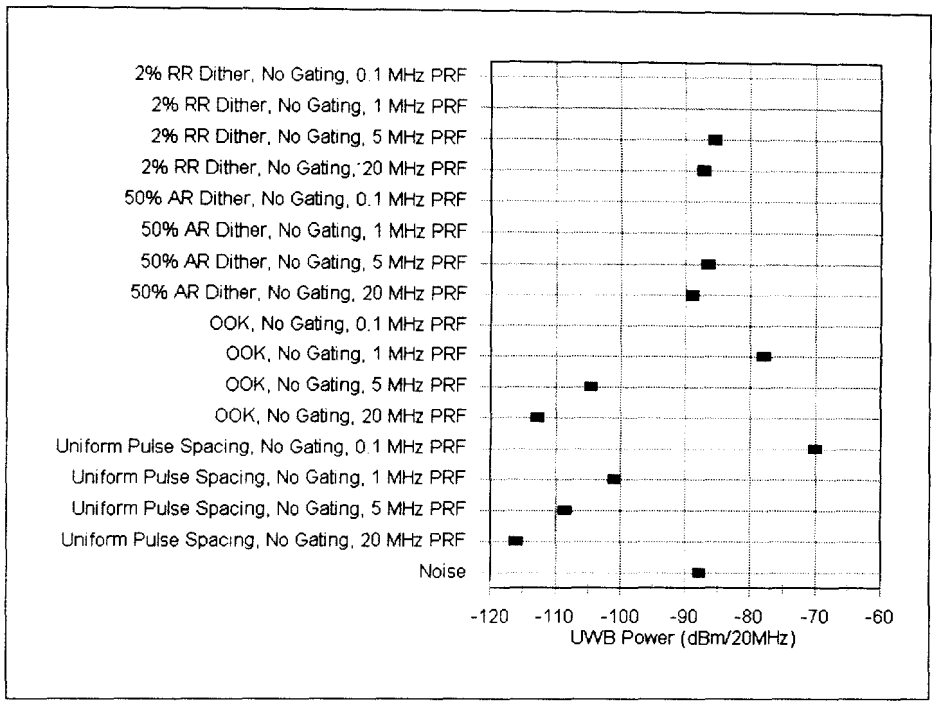

Figure 6.2.1. Non-gated UWB signal vs. signal power at BL (Rx 1).

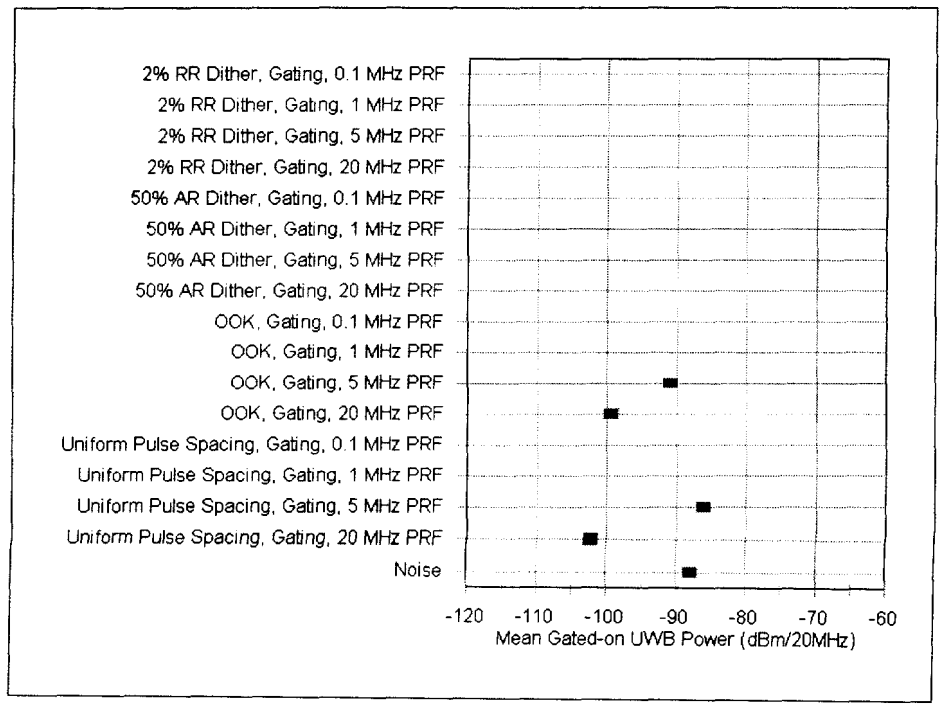

Figure 6.2.2. Gated UWB signal vs. signal power at BL (Rx 1).

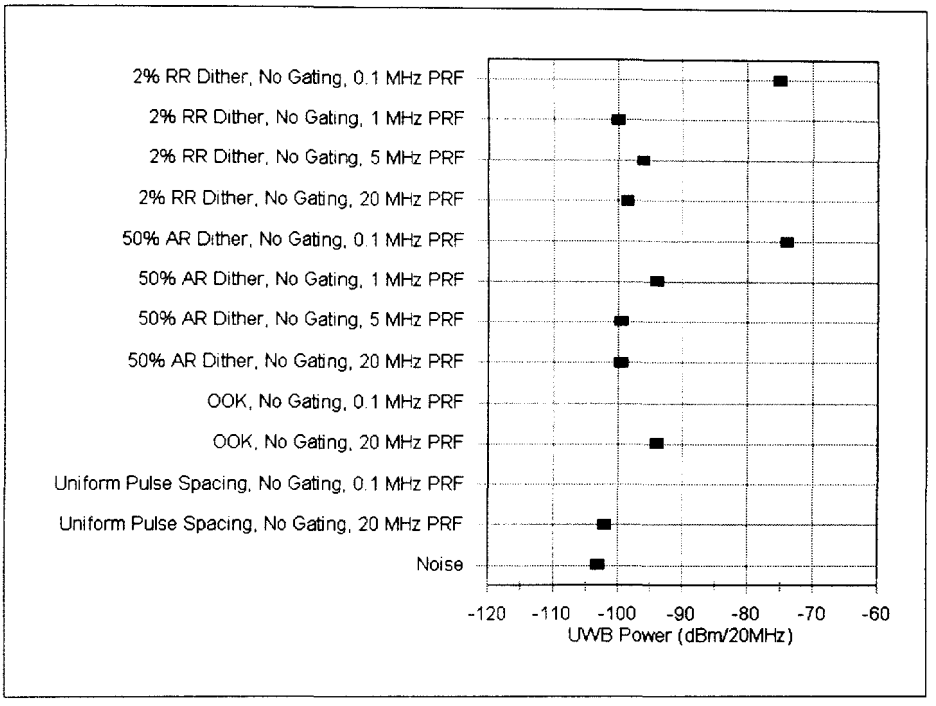

Figure 6.2.3. Non-gated UWB signal vs. signal power at BL (Rx 2).

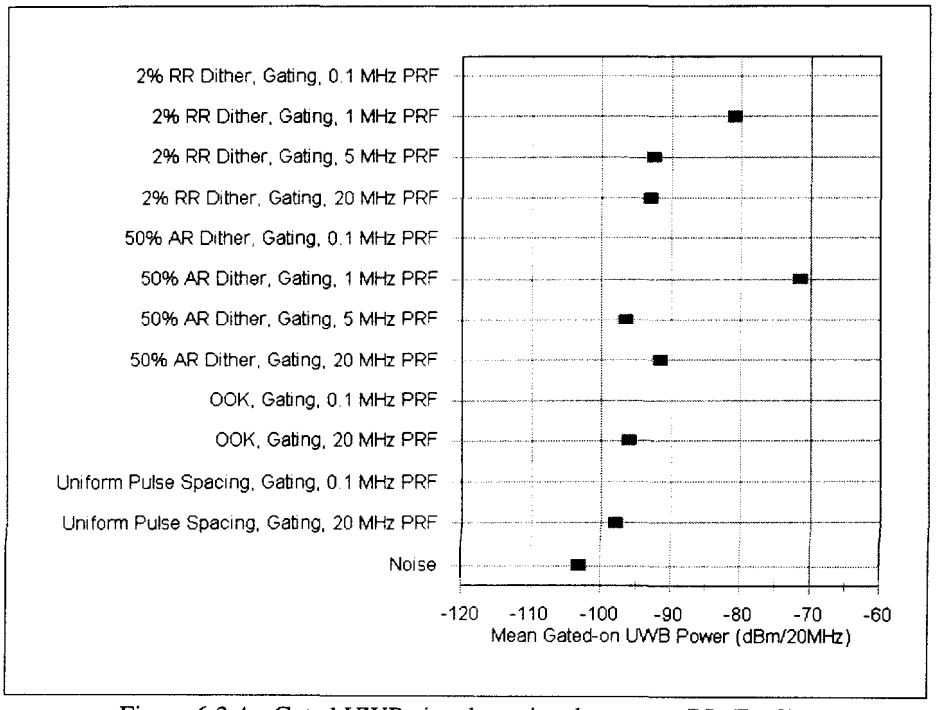

Figure 6.2.4. Gated UWB signal vs. signal power at BL (Rx 2).

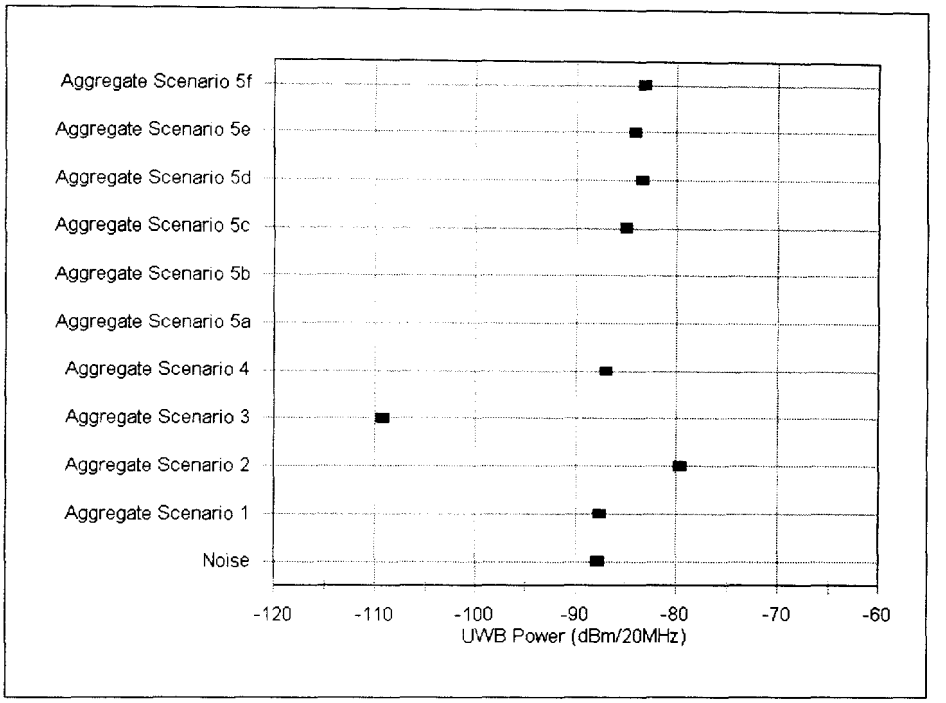

Figure 6.2.5. Aggregate UWB signal vs. signal power at BL (Rx 1).

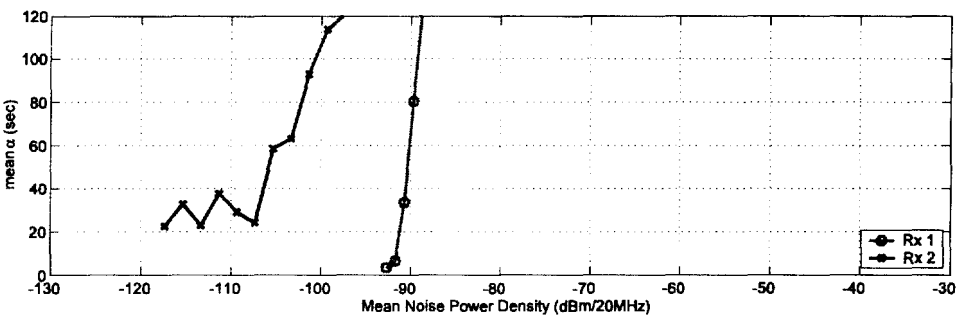

Figure 6.2.6. RQT of GPS receivers when exposed to Gaussian-noise interference.

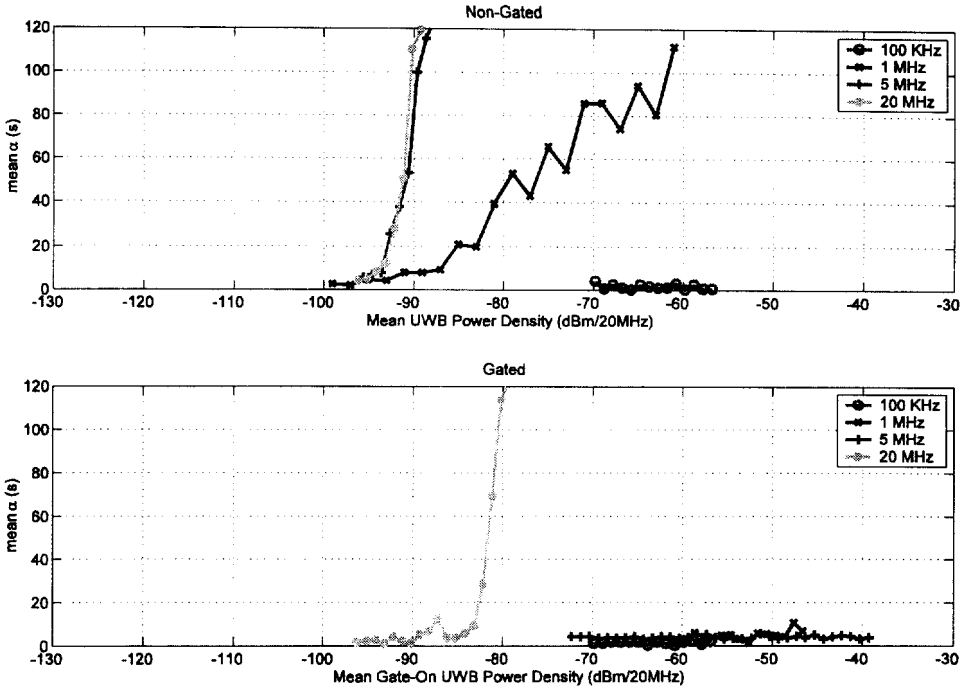

Figure 6.2.7. RQT of Rx 1 when exposed to 2%-RRD UWB interference.

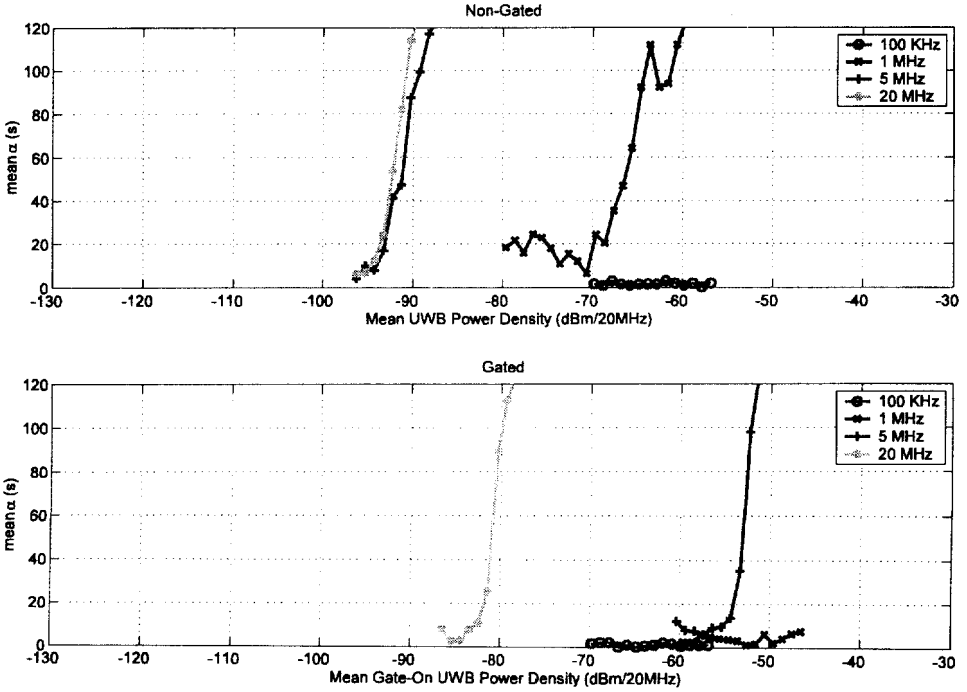

Figure 6.2.8. RQT of Rx 1 when exposed to 50%-ARD UWB interference.

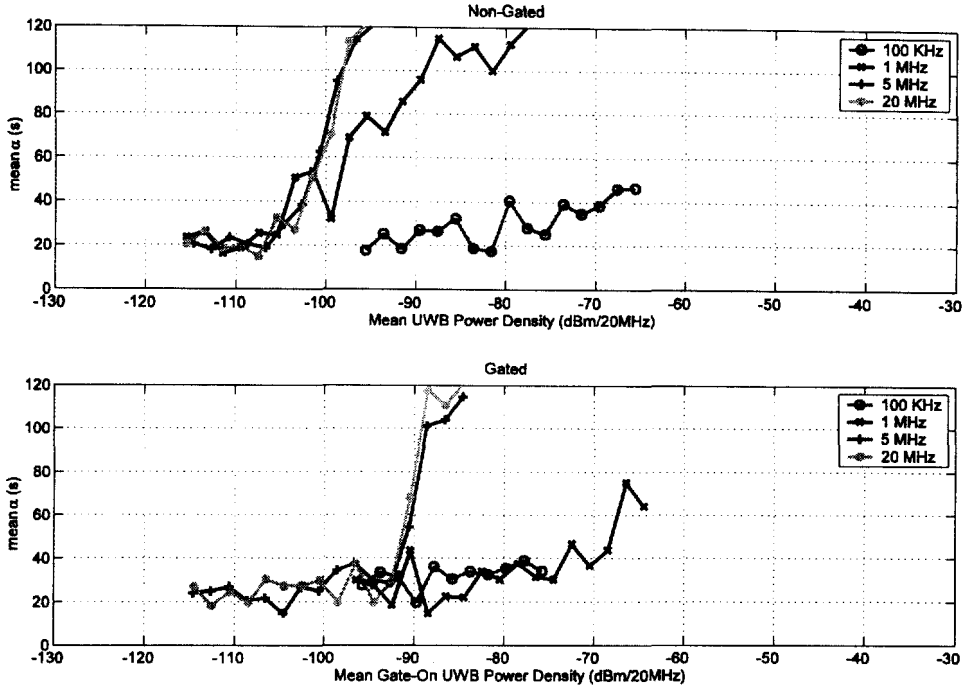

Figure 6.2.9. RQT of Rx 2 when exposed to 2%-RRD UWB interference.

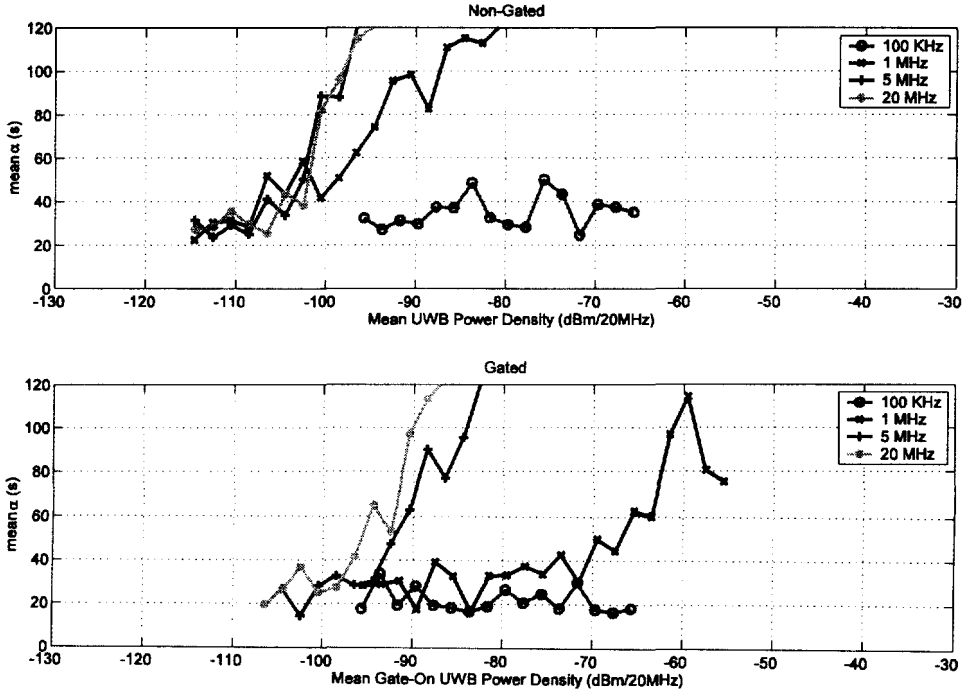

Figure 6.2.10. RQT of Rx 2 when exposed to 50%-ARD UWB interference.